Journal Pre-proof

Curing kinetics of acrylate-based and 3D printable IPNs

Osman Konuray<ce:contributor-role>Writing-review and editing) (Visualization)<ce:contributor-role>Investigation, Data curation)<ce:contributor-role>Writing- original draft, Conceptualization) (Methodology) (Software), José M. Salla (Data curation)<ce:contributor-role>Writing- original draft), José M. Morancho (Visualization) (Investigation), Xavier Fernández-Francos (Data curation)<ce:contributor-role>Writing- original draft) (Conceptualization) (Methodology) (Software), Montserrat García-Alvarez (Visualization) (Investigation), Xavier Ramis (Project administration)<ce:contributor-role>Writing-review and editing) (Supervision) (Data curation)<ce:contributor-role>Writing- original draft) (Conceptualization) (Methodology) (Software)

PII: S0040-6031(20)30669-9

DOI: https://doi.org/10.1016/j.tca.2020.178754

Reference: TCA 178754

To appear in: *Thermochimica Acta*

Received Date: 30 June 2020

Revised Date: 11 August 2020

Accepted Date: 13 August 2020

Please cite this article as: Konuray O, Salla JM, Morancho JM, Fernández-Francos X, García-Alvarez M, Ramis X, Curing kinetics of acrylate-based and 3D printable IPNs, *Thermochimica Acta* (2020), doi: https://doi.org/10.1016/j.tca.2020.178754

Curing kinetics of acrylate-based and 3D printable IPNs

Osman Konuray[1], José M. Salla[1], José M. Morancho[1], Xavier Fernández-Francos[1], Montserrat García-Alvarez[2], Xavier Ramis[1*]

[1] Thermodynamics Laboratory, ETSEIB Universitat Politècnica de Catalunya, Av. Diagonal 647, 08028, Barcelona, Spain

[2] Department of Chemical Engineering, ETSEIB Universitat Politècnica de Catalunya, Av. Diagonal 647, 08028, Barcelona, Spain

* Corresponding author: Tel.: +34 934016592; fax: + 34 934017389

E-mail address: ramis@mmt.upc.edu

Graphical abstract

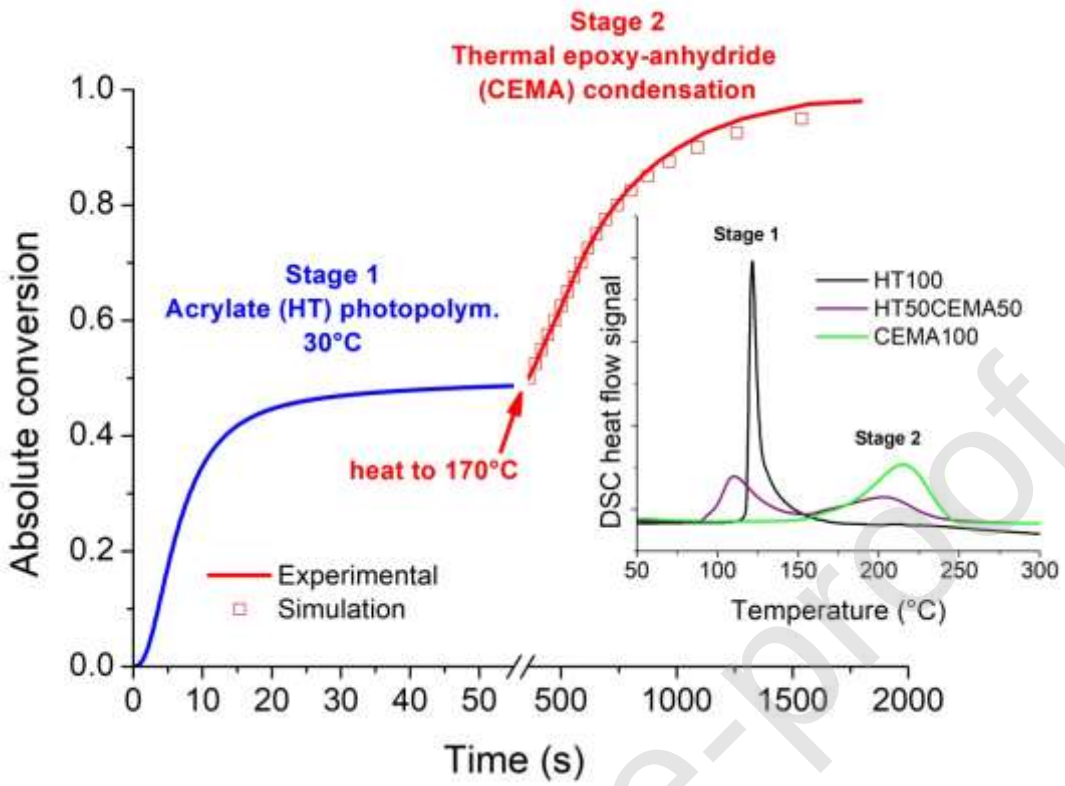

Highlights

- Dual-curing kinetics of a ternary acrylate-epoxy-anhydride mixture is studied.
- Acrylate UV photopolymerization is followed by thermal epoxy-anhydride condensation
- Calculated kinetic parameters corroborate the dual nature of the curing
- Formulations are potentially useful for stereolithography
- Addition of a thermal radical initiator allows also a purely thermal curing process

Abstract

In this work, the kinetics of curing of a new family of interpenetrating polymer networks (IPNs) obtained by co-formulation of a photocurable acrylic resin with a thermocurable epoxy/anhydride mixture is studied. The first curing stage is an acrylate free-radical photopolymerization at ambient temperature, and the second curing stage is an epoxy-anhydride copolymerization initiated with a nucleophilic tertiary amine at higher temperatures. The presence of a diperoxyketal thermal radical initiator added to the liquid formulation facilitates uniform and complete acrylate conversion during thermal second curing stage and opens the possibility of curing the same materials by thermal curing only. The thermal curing kinetics was studied by integral isoconversional and model fitting procedures, whereas photocuring kinetics was satisfactorily fitted to a first order expression. Thermal curing and storage stability at room temperature were successfully simulated by using the isoconversional kinetic parameters. These ternary formulations have potential as 3D printable thermosets.

Keywords

Acrylate; epoxy; dual-curing; thermosets; stereolithography

1 Introduction

An in-demand and efficient additive manufacturing method, stereolithography (SL) affords high spatial resolutions [1], relatively short build times and can accommodate a broad range of chemistries [2,3]. Although SL initially was used as an efficient prototyping tool, with the recent advances in polymer chemistry, it shows potential in customized manufacturing of high added value materials such as orthodontic plastic inserts [4,5], scaffolds for tissue engineering [6,7], electronics [8], soft robotics [9], bioinspired graded materials [10] and shape memory materials [11].

The majority of SL resins are based on acrylate chemistry, which results in final materials with polymerization-induced shrinkage [12] that have poor thermal and mechanical performance [13]. To alleviate these problems, the use of different fillers, such us fused silica, carbon fibers and other nanofillers, have been reported [14,15]. However, the opacity of the fillers leads to poorly cured materials, even after postcuring in a UV-oven. Moreover, it is known that the light penetration and cure depth are controlled by the photoabsorptivity of the resin, with an exponential decay in light intensity, leading to a gradient in conversion within each printed layer, which can range from almost complete cure to barely gelled material. This variation causes a property gradient within each layer and is responsible for the poor properties of the final material compared with the bulk materials. Again, postcuring would increase the degree of conversion, but it still would not achieve a complete and homogeneous cure [16].

Many cured commercial photoresins have low mechanical properties at room temperature since the materials are partially relaxed under operation conditions due to their low T_gs. A slight increase in T_g can have a dramatic effect on mechanical properties if the partially relaxed material reached the glassy state at the working temperature [17]. Although vitrification is not the main drawback in SL technology, some photoresins with

final glass transition temperatures (T_g) much higher than room temperature can vitrify during photocuring, leaving the cure incomplete [18-20]. Full cure could be achieved in a subsequent thermal postcuring process at a higher temperature in order to devitrify the material, providing a suitable radical thermal initiator was included in the formulation.

Acrylate radical polymerization has another disadvantage, namely, the inhibition of curing by oxygen, which can be alleviated using different strategies such as working in an inert environment, increasing the photoinitiator content, increasing the duration and the intensity of light exposure and the addition of oxygen scavengers [21]. This latter strategy may be interesting when these oxygen scavengers are part of the reagents, as in the case of tertiary amines added as initiators or formed during curing [22].

Few articles address the use of dual-curing methodology to mitigate some of the drawbacks aforementioned. Griffini et al. [23] achieve an increase from 37 to 103 ºC and from 2.5 to 3 GPa in calorimetric T_g and storage modulus, respectively, by adding 50 % by weight of DGEBA/DYCY mixture to a bisphenol A ethoxylate diacrylate. Kuang et al. [24] developed a novel ink for high-speed 3D printing, which contained a photocurable triacrylate and a thermally curable epoxy/anhydride mixture. It reached high printing speed and resolution, low volume shrinkage and good mechanical properties, but glass transition temperature was barely modified.

In two publications [13,14], new dual-cure acrylate-based resins were described that can be thermally post-processed with the help of a thermal initiator. Both authors recorded mechanical property improvements, high conversions and tack-free surface.

In an earlier manuscript [17], we presented a new dual-curable SL resin, composed of a cycloaliphatic epoxy monomer and a radical thermal initiator mixed into a commercial multi-acrylate resin. A sequential curing scheme was employed wherein acrylate free-radical photopolymerization at ambient temperature was followed by an

cationic epoxy homopolymerization at higher temperatures. During second stage the unreacted double bonds thermally reacted to yield fully cured materials. These new materials have superior thermomechanical properties due to two factors: the incorporation of the more densely crosslinked epoxy network and the thermally facilitated increased conversion of acrylates. In another recent manuscript [25], we described epoxy-anhydride doped poly-acrylate 3D printed materials. These new dual-curable thermosets had wide ranges of properties at both curing stages, with epoxy-rich formulations exhibiting nanoscale phase separation. In comparison with the neat acrylate, doped formulations had increased T_g and modulus at room temperature, as a consequence of their glassy state.

Dean and Cook studied interpenetrated networks (IPNs) based on radical polymerization of methacrylates combined with epoxy-anhydride copolymerization [26], vinyl esters combined with epoxy-amine condensation [27] or imidazole-cured epoxy [28]. The authors described complex interactions between the reactive components of the mixture in terms of curing kinetics and extent of reaction, depending on the type of radical initiator and curing agent for the epoxy, and described that the curing sequence could have a significant effect on the thermal-mechanical properties and morphology of final materials.

The study of the curing kinetics is a fundamental tool to analyze dual-curing systems [29,30] as well as to establish safe processing and storage conditions in order to ensure controlled curing sequence in formulations containing several reagents and initiating systems. This is especially important taking into account the complex interactions between the different components that may lead to complex kinetic effects. To the best of our knowledge, there is no such treatment of dual-curing kinetics in the context of SL resins.

Taking all this into account, in the present publication we present the curing kinetics and thermal characterization of a new family of acrylate-based SL resins. The first curing stage was radical photopolymerization of acrylate groups at 30 ºC and the second stage was epoxy-anhydride condensation catalyzed by 4-(dimethylamino)pyridine as anionic initiator, along with the thermal polymerization of unreacted acrylate groups initiated by 1,1-di(t-amylperoxy)-cyclohexane. The extent and rate of both curing stages were studied by calorimetry and FTIR spectroscopy. The kinetics of thermal curing was studied by integral isoconversional dynamic/isothermal procedure and by autocatalytic model fitting. Combining both procedures, the kinetic triplet, activation energy, pre-exponential factor and conversion function were determined. The rate constant of the acrylate photocuring was determined by fitting conversion data to a first order kinetic model.

2 Experimental methods

2.1 Materials

The SL resin mixture, with trade name Spot-HT (HT hereafter) (Spot-A Materials, Barcelona, Spain) is a mixture of aliphatic and urethane acrylates with a double bond equivalent of 283.4 g/C=C and a photoinitiator which has an absorption range in the UV-visible region of the spectrum. Cycloaliphatic epoxy resin 3,4-epoxycyclohexylmethyl -3′,4′-epoxycyclohexanecarboxylate (CE), with trade name CYRACURE UVR-6105 (IGM Resins, Barcelona, Spain) with an epoxy equivalent of 130 g/ee and hexahydro-4-methylphthalic anhydride (MA, Sigma-Aldrich) with an anhydride equivalent of 168.19 g/ae were used as epoxy and anhydride comonomers, respectively. The epoxy monomer was dried under vacuum at 80°C for two hours and stored into a desiccator before use. 4-(dimethylamino)pyridine (DMAP, Sigma Aldrich) and 1,1-di(t-amylperoxy)-cyclohexane with trade name LUPEROX 531M60 (LUP hereafter) (ARKEMA,

Colombes, France) were used as anionic initiator and peroxidic radical initiator, respectively.

2.2 Sample preparation

First of all, a stoichiometric epoxy-anhydride mixture was prepared and coded as CEMA100. Also, neat HT with an added 0,25% by weight of LUP (by manual mixing at room temperature), was coded as HT100. Mixtures of different compositions were mixed at room temperature and were coded as HTxCEMAy, where x and y indicate weight percentages (%) of HT100 and CEMA100, respectively. DMAP was added at 0.025% by weight (based on total formulation) to the mixtures and samples were kept under magnetic agitation at 30 ºC for 10 min until complete dissolution of DMAP. All samples were stored under refrigeration. HT100 and all HTxCEMAy samples were stored in aluminum foil wrapped vials to prevent premature activation of acrylate polymerization. For simplicity, the initiator amounts will be omitted in referring to the samples. The following formulations were studied: HT100, HT75CEMA25, HT50CEMA50, HT25CEMA75 and CEMA100.

2.3 Experimental techniques

The photocurable samples were UV cured at 30 ºC in a Mettler DSC-821e calorimeter appropriately modified with a Hamamatsu Lightningcure LC5 (Hg-Xe lamp) with two beams, one for the sample side and the other for the reference side. Samples of ca. 3 mg were cured in open aluminum pans in a nitrogen atmosphere. Two scans were performed on each sample to subtract the thermal effect of UV irradiation from the photocuring experiment, each one consisting of 1 min of temperature conditioning, 6 min of irradiation, and an additional 1 min without UV light. The light intensity was calculated by irradiation of graphite-filled pans on only the sample side. UV-cured samples were postcured on a Mettler DSC3+ calorimeter equipped with an intra-cooler. The UV-cured

samples were analyzed from -80 to 250 ºC at 10 ºC min^{-1} to determine the intermediate T_g (T_{gint}) and the residual heat of the second stage. After this, a second dynamic run at 10 ºC/min was carried out to determine the ultimate T_g ($T_{g\infty}$). Both thermal analyzers were calibrated using an indium standard (heat flow calibration).

For other calorimetric measurements, we used a Mettler DSC 3+ calorimeter. Samples of ca. 10 mg were placed in aluminum pans and were scanned under nitrogen atmosphere in the analyzer using various temperature programs depending on the type of measurement. Dual curable samples were thermally cured from -80 ºC to 300 ºC at 10 ºC/min to determine T_g of uncured samples (T_{g0}) and the total reaction heat (of the two curing stages). For kinetics studies, non-isothermal curing was performed at 2.5, 5, 10 and 20 ºC/min up to 300 ºC for the dual curing and for the second curing stage of intermediate materials. For some formulations isothermal curing was performed at temperatures of 100, 110 and 100 ºC (stage 1) and 130, 150, 170 and 190 ºC (stage 2).

Partial and total reaction heats were obtained by integration of the calorimetric signal, dh/dt. For each stage, relative conversion, α, was determined by dividing the reaction heat released up to a temperature or time to the total reaction heat released during the experiment. Absolute conversion of each monomer was determined as the product of relative conversion and the mole fraction of the monomer in the formulation.

The T_g of the uncured, intermediate and final material were determined from dynamic scans at 10 °C min^{-1} (as described above) and taken as the half-way point in the jump in the heat capacity step, following the DIN 51007 method in the STARe software by Mettler. The estimated error of the determination of T_g was ± 1°C.

A Brucker Vertex 70 FTIR spectrometer equipped with an attenuated total refection (ATR) accessory (Golden gate™, Specac Ltd) which is temperature controlled (heated single-reflection diamond ATR crystal) was used to monitor the evolution of acrylate and

anhydride groups during isothermal dual curing of the formulations. Real-time spectra were recorded at 30 °C (stage 1) and 170 ºC (stage 2) in absorbance mode with a resolution of 4 cm^{-1} and a wavelength ranging from 400 to 4000 cm^{-1}, averaging 20 scans for each spectrum. A Hamamatsu Lightning Cure LC5 (Hg-Xe lamp) with one beam conveniently adapted to an ATR accessory was used to irradiate the samples during the first curing stage. A wire-wound rod was used to set a sample thickness of 25 μm. The dual curing process was performed in a similar way to DSC curing, 6 minutes of UV-irradiation at 30ºC followed by 2 hours at 170 ºC. Curing times and temperatures of stage 2 were selected, as will be showed later, by simulation using DSC kinetic data. Conversions of intermediate and final materials were also checked by real time FTIR at 30 ºC. The spectra were corrected taking into account the dependence of the penetration on the wavelength and normalized using the area of the carbonyl ester band at 1730 cm^{-1} (stage 1) and the area of the saturated C-H stretching at 2930-2870 cm^{-1} (stage 2). The peaks at 1407 cm^{1} (CH_2 scissor deformation mode) and 1862-1785 cm^{-1} (carbonyl stretching) were used for monitoring of acrylate and anhydride groups, respectively. Bands at 810 and 1636-1620 cm^{-1} for acrylate, 894 cm^{-1} for anhydride groups and 740 cm^{-1} for epoxy groups were also monitored, but not used for quantification. Conversions were determined as:

$$\alpha = 1 - \frac{\frac{A_t^i}{A_t^{ref}}}{\frac{A_0^i}{A_0^{ref}}} \qquad (1)$$

where A_t is the absorbance of the band of interest (i=1407 or 1862-1785 cm^{-1}), A_{ref} the absorbance of the reference band, and subscripts *0* and *t* represent initial spectrum and reaction time, respectively.

3 Kinetic theory

3.1 Photocuring

Free radical polymerization of double-bonds proceeds via a chain-growth mechanism with the following stages: (a) dissociation of the initiator to form initiating radicals, (b) initiation where a monomer is attached to the radical initiator to form an active radical, (c) propagation by growth of the active chain (free radical) through sequential addition of monomers and (d) termination by disproportional coupling between radicals. In this mechanism, initiation is the rate-determining stage. In contrast to the step-growth polymerization, in this mechanism the functional groups can only react with the active sites situated at the end of the growing chains and high-molecular-weight polymer chains are formed in the early stages of the process.

Although the detailed kinetic study of the free radical polymerization can be rather complex, it is generally accepted that photopolymerization is first-order in the initial stage of the polymerization. Taking this into account and assuming continuous irradiation, pseudo-steady state initiator concentration, and bimolecular termination, the rate constant of polymerization can be defined as [31,32]:

$$-\frac{d[M]}{dt} = k_p \left(\frac{\phi_i \cdot I_a}{k_t} \right)^{1/2} [M] \qquad (2)$$

Or in a more compact way as:

$$-\frac{d[M]}{dt} = k[M] \qquad (3)$$

where k is an apparent kinetic constant, k_p and k_t are the propagation and termination rate constants, [M] is the concentration of monomer (acrylate), and $\phi_i \cdot I_a$ is the initiation rate expressed in terms of quantum yield of the photolysis (ϕ_i) and intensity absorbed (I_a).

Reordering and rewriting Eq. 3 in terms of conversion, the following equation is obtained:

$$\ln(1-\alpha) = -k\,t \qquad (4)$$

The apparent rate constant *k* at a given temperature can be obtained from the slope of the representation of ln(1-α) against time *t*.

In this work Eq. (4) was used to determine the *k* of stage 1 (UV-induced photopolymerization) at 30 ºC of the different formulations. Activation energy and other kinetic parameters were not determined.

3.2 Thermal curing

Isoconversional and model fitting methods were used to determine the kinetic parameters in accordance with the ICTAC Kinetics Committee recommendations and the results obtained in previous works [33-36].

Isothermal curing kinetics have been analyzed by means of an integral isoconversional method, based on the assumption that reaction rate at constant conversion is a function of temperature only, using the following equation

$$\ln t_{\alpha,i} = \ln\left[\frac{g(\alpha)}{A_\alpha}\right] + \frac{E_\alpha}{RT_{\alpha,i}} \qquad (5)$$

where A_α the frequency factor, E_α the activation energy and $t_{\alpha,i}$ the time to reach a given relative conversion at temperature $T_{\alpha,i}$. $g(\alpha)$ is the integral obtained from a function of the relative degree of conversion $f(\alpha)$:

$$g(\alpha) = \int_0^\alpha \frac{d\alpha}{f(\alpha)} \qquad (6)$$

The values of kinetic parameters E_α and $\ln[g(\alpha)/A_\alpha]$, are determined from the slope and intercept at the origin of the plot $\ln t_{\alpha,i}$ versus $1/RT_{\alpha,i}$ respectively (Eq. (5)). If the

reaction model $g(\alpha)$ is known, the corresponding pre-exponential factor can be calculated for each conversion.

The kinetics of non-isothermal curing has been analyzed by means of an integral isoconversional method, namely Kissinger-Akahira-Sunose (KAS), based on the Coats-Redfern approximation for the solution of the so-called temperature integral [37,38]:

$$\ln\left(\frac{\beta_i}{T_{\alpha,i}^{\ 2}}\right)=\ln\left[\frac{A_\alpha R}{g(\alpha)\,E_\alpha}\right]-\frac{E_\alpha}{RT_{\alpha,i}} \qquad (7)$$

The values of dynamic kinetic parameters E_α and $\ln[A_\alpha R/g(\alpha)E_\alpha]$, are determined from the slope and intercept at the origin of the plot $\ln(\beta_i/T_{\alpha,i}^{\ 2})$ versus $1/RT_{\alpha,i}$ respectively. Once the activation energy is determined, it is possible to determine the parameter $\ln[g(\alpha)/A_\alpha]$ If the reaction model $g(\alpha)$ is known, the corresponding pre-exponential factor can also be easily calculated.

Given that both Eq.(5) and (7) are integral methods, the kinetic parameters determined from these expressions are equivalent. It is possible to simulate isothermal curing based on non-isothermal data starting from the parameters E_α and $\ln[g(\alpha)/A_\alpha]$, that is, without needing to know the kinetic model represented by the integral function $g(\alpha)$. This methodology, used in this work, is very useful when simulation is required outside the range of the experimental data or the analysis of the curing process under isothermal conditions is difficult.

In order to determine the reaction model, equations (5) and (7) were rearranged into equations (8) and (9) respectively, as follows:

$$\ln\frac{t}{g(\alpha)}=\ln\left[\frac{1}{A}\right]+\frac{E}{RT} \qquad (8)$$

$$\ln\left(\frac{g(\alpha)\beta_i}{T^2}\right)=\ln\left[\frac{AR}{E}\right]-\frac{E}{RT} \qquad (9)$$

These expressions constitute composite integral methods that make it possible to determine the kinetic triplet from the whole conversion range and all isothermal temperatures or heating rates. Representation of $\ln(t/g(\alpha))$ or $\ln(g(\alpha)\beta_i/T^2)$ against $1/RT$ throughout the whole conversion range and set of experiments produce a single straight line with a slope equal to the isoconversional *E* or *–E*, if the kinetic model $g(\alpha)$ is right. The preexponential factor *A* is determined from the intercept at the origin of Eq. (8) and (9).

It is usually accepted that epoxy-anhydride condensation and thermal acrylate free-radical polymerizations can be modelled using autocatalytic models. In the present work, both curing stages were fitted to an autocatalytic kinetic model with $n + m = 2$, where *n* and *m* are the partial orders of reaction [34-36,39,40]. Eqs. (10) and (11) show $g(\alpha)$ and $f(\alpha)$ functions, for the autocatalytic kinetic model used:

$$g(\alpha) = \frac{1}{1-m}\left(\frac{\alpha}{1-\alpha}\right)^{1-m} \qquad (10)$$

$$f(\alpha) = \alpha^m (1-\alpha)^{2-m} \qquad (11)$$

The sequential character of the dual curing process enables the individual study of each curing stage. Stage 1 UV-induced photopolymerization was studied at 30ºC assuming an n^{th}order model. Thermal curing of neat stage 1 and 2 and dual formulations were studied by isoconversional procedures followed by model fitting, under isothermal and non-isothermal conditions. In general, non-isothermal experiments were preferred, given the difficulties often faced in the isothermal characterization of the curing process by DSC. Nevertheless, FTIR experiments were performed in isothermal conditions.

4 Results and discussion

4.1 Preliminary characterization of HTxCEMAy formulations

Dual curing analysis

First of all, we studied the sequential and isothermal curing of a HT50CEMA50 formulation. Figure 1 (stage 1, UV at 30ºC) shows some spectra collected during photocuring at 30 ºC of formulation HT50CEMA50. The complete disappearance of acrylate groups can be observed, whereas anhydride and epoxy appear to not have reacted (region not shown). In Figure 2 the real-time spectra of thermal curing at 170 ºC of neat CEMA100 is presented. The virtually complete disappearance of the epoxy and anhydride bands is shown.

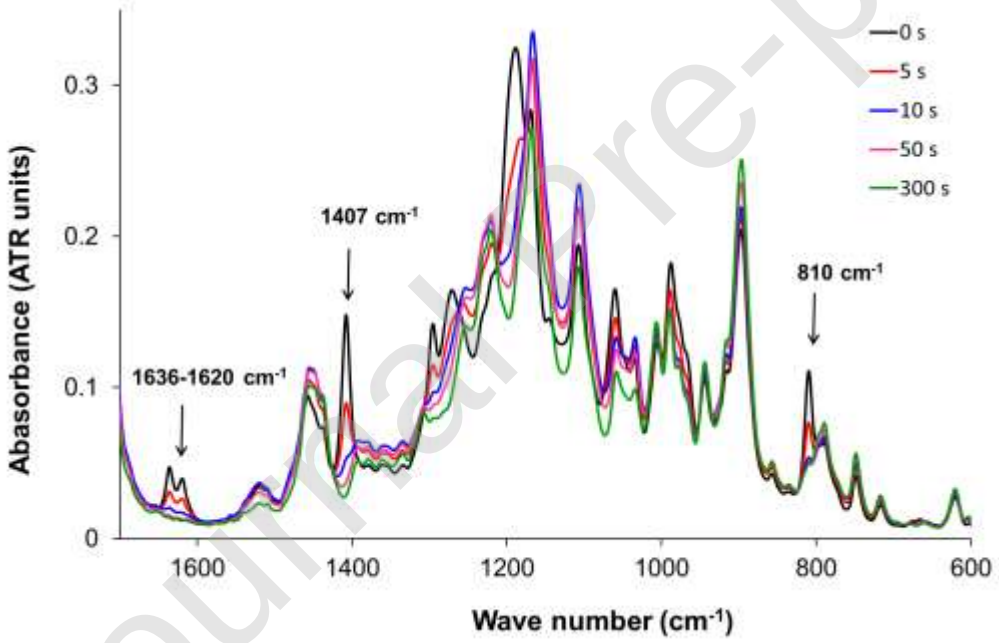

Figure 1. Evolution of FTIR spectra at 30 ºC for HT50CEMA50 monitored during radical acrylate photopolymerization.

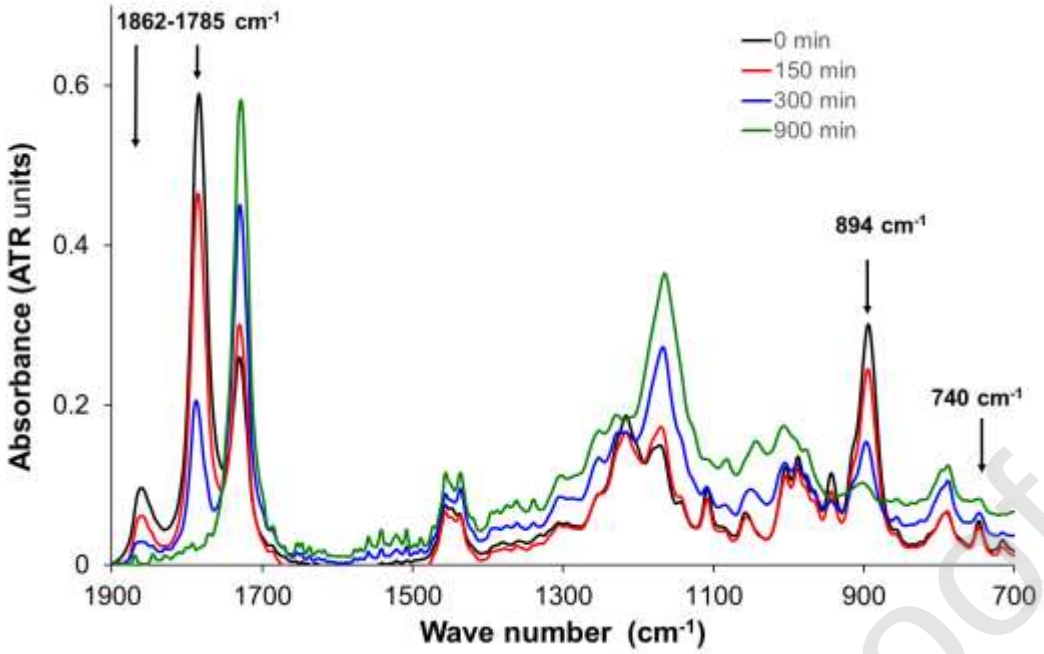

Figure 2. Evolution of FTIR spectra at 170 ºC for CEMA100 monitored during epoxy-anhydride copolymerization.

Figure 3 shows the absolute conversions achieved during the two consecutive curing stages in FTIR: 6 min at 30 ºC under UV irradiation (acrylate polymerization) followed by 60 min at 170 ºC (epoxy anhydride copolymerization). It can be observed that both curing stages reach completion, indicated by a fractional conversion of 0.5 and 1 at the end of the first and the second stages, respectively. During stage 1, anhydride and epoxy remains unreacted and stage 2 remains dormant until the sample is heated to 170 °C upon which the epoxy-anhydride reaction begins in a controlled manner. Figure 3 also shows the agreement between the DSC and FTIR data and the accurate simulation of stage 2 using non-isothermal parameters. As will be discussed later, simulation will be considered more accurate than isothermal curing in DSC. Moreover, Figure 3 serves also as confirmation of the dual character HTxCEMAy formulations with a well-defined curing sequence, which is controlled mainly by the irradiation of the formulation at room temperature.

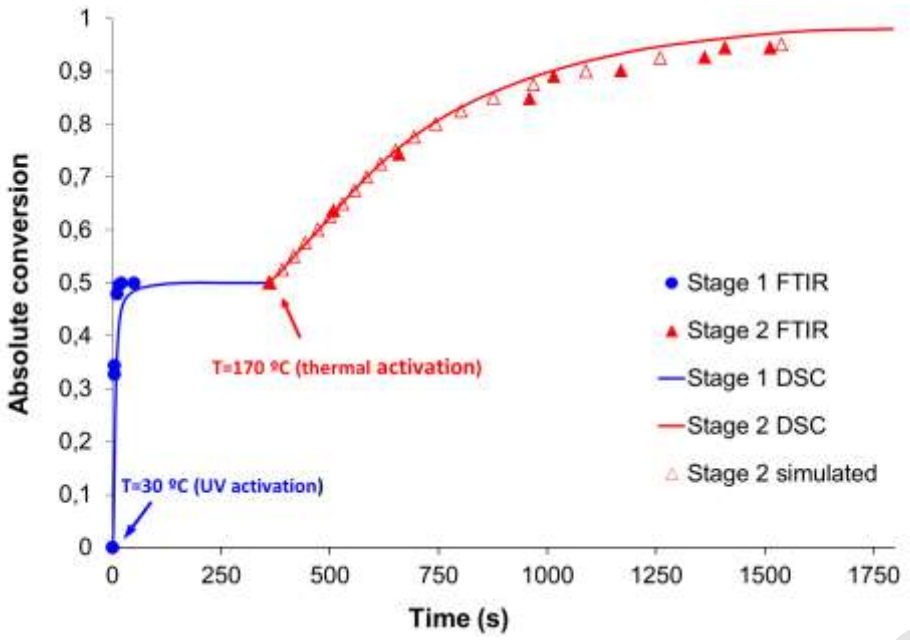

Figure 3. FTIR and DSC absolute conversion during isothermal curing at 30 ºC (stage 1, acrylate) and later at 170ºC (stage 2, anhydride) for HT50CEMA50. Simulation of stage 2 using non-isothermal kinetic parameters is also shown.

We decided to analyse if the HTxCEMAy formulations could be processed following controlled curing sequences in the absence of UV light. Figure 4 shows the DSC traces and conversion-temperature plots of different formulations cured dynamically at 10 ºC/min. Again, a well-defined dual curing sequence can be observed, with two clearly separated exothermic events. By comparison with the neat formulations, these can be unequivocally attributed to acrylate polymerization (low *T*) and to the epoxy-anhydride condensation (high *T*). This is also made evident looking at the conversion curves (see Figure 4 *inset*), showing two well-defined curing steps which are proportional to the theoretical contribution of each one of the curing reactions, assuming that the heat released per double bond and epoxy ring are similar.

Figure 4 also shows the effect of each stage on the other. Stage 1 reaction rate increases sharply (especially remarkable is the case of pure HT100) at high percentages of HT content, despite the shift of the curves at higher temperatures. The DSC profile of HT100 suggests that a minimum temperature of 100 ºC is necessary for the thermal

decomposition of LUP in the absence of DMAP, but once this occurs, the reaction is very fast. At low HT contents, the reaction begins at lower temperatures due to the accelerating effect of DMAP, which can promote the decomposition of LUP via chemical reduction (redox mechanism) [41]. DMAP bears a dimethylamino moiety that is common in many tertiary aromatic amines used for the acceleration of free-radical polymerization processes [42].

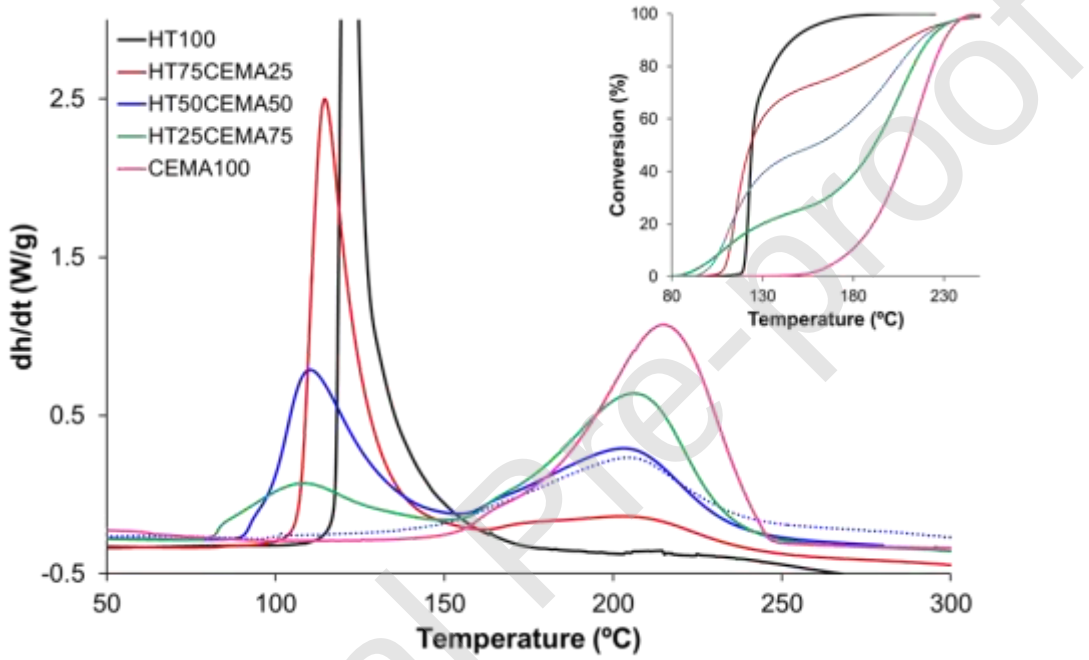

Figure 4. DSC thermograms corresponding to the dynamic curing at 10 ºC/min of HTxCEMAy formulations. Maximum of HT100 appeared close to 6 W/g. Blue dashed line shows the dynamic postcuring of HT50CEMA50 after 6 min of UV irradiation. Inset shows conversion-temperature plots.

However, the effect of DMAP may be more complex given that it is a nucleophilic initiator that can promote the Michael addition to acrylates. As seen in the Scheme 1, the nucleophilic addition of the pyridinic nitrogen of DMAP to the acrylate double bond (a) would lead to a reaction product with a positive charge that is stabilized within the aromatic ring or by the formation of other resonant structures (b). This reaction product would not have the reducing potencial required for the redox mechanism in order to promote the formation of radicals from LUP [43]. With increasing HT content, the

probability of Michael addition of DMAP to an acrylate double bond increases, therefore leaving a smaller amount of free DMAP available for the redox activation. In contrast, at lower HT content the lower likelihood of Michael addition results in a significant contribution of free DMAP to the redox activation of LUP, resulting in a faster activation of the acrylate homopolymerization at a lower temperature.

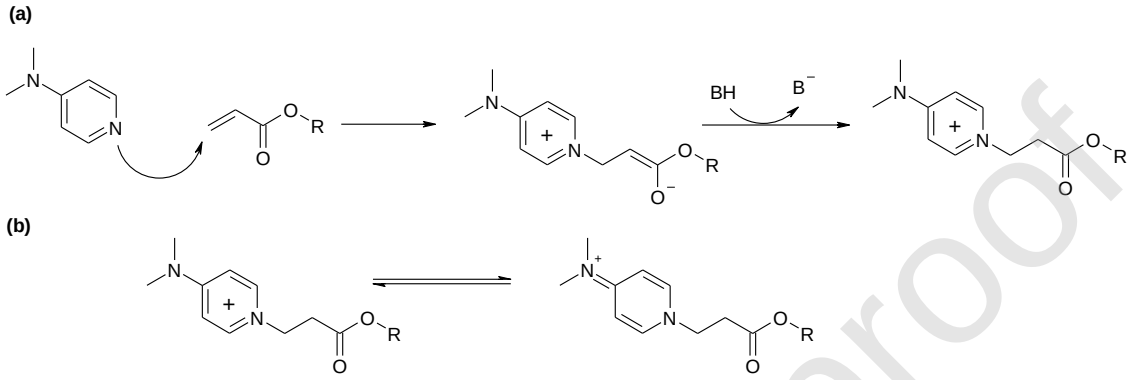

Scheme 1. (a) Nucleophilic addition of DMAP to an acrylate double bond and (b) resonant structures of addition product.

Stage 2 is hardly influenced by the relative HT/CEMA content, showing a slight shift to lower temperatures when HT content increases. If there was a dilutional effect of the acrylate on the concentration of epoxy and anhydride groups and the catalyst, the result would be opposite. On the contrary, the results suggest that the apparent concentration of reactive groups and initiating species would be similar to that of the neat system, indicating that the formed acrylate network is not acting as a diluent and the components of the epoxy formulation are phase-separated after the end of stage 1. Indeed, Dean and Cook reported a similar effect for the sequential curing of methacrylate/epoxy IPNs [26]. Bonnet et al. studied the effect of phase-separation on the reaction rate of epoxy-amine thermosets blended with thermoplastics [44], showing an increase in reaction rate when reaction-induced phase separation takes place, caused by an increase in the concentration of reactive groups in the epoxy-rich phase. Indeed, in a recent work [25] we reported that

dual-curable HTxCEMAy formulations with controlled curing sequence produce phase separated materials at the nano-scale. The present results suggest that there is already some phase separation present in the system at the end of the first curing stage. Furthermore, the epoxy-anhydride reaction is even apparently accelerated when increasing HT content. This further enhancement of reaction rate can result from a positive interaction between the different components of the mixture, such as the formation of active species by nucleophilic addition of DMAP to acrylate groups, which takes place rapidly at room temperature [43] in combination with the presence of proton donors, producing species that can activate the epoxy-anhydride reaction (see Scheme 1 (a)).

Figure 4 also includes the postcuring (by DSC) of HT50CEMA50 after UV curing at 30 ºC (dashed line). It can be observed that this DSC peak matches in position and size with stage 2 of the dual curing, indicating than during stage 1, epoxy-anhydride copolymerization does not take place. Again, the effective control of the curing sequence (UV curing + thermal curing) of HTxCEMAy formulations is confirmed by these results.

Thermal properties

Table 1 shows some characteristic parameters of curing and the glass transition temperatures of uncured, intermediate and fully cured HTxCEMAy materials. The similarity between the experimental reaction heats (values close to 100-110 kJ/ee or kJ/C=C) and those reported for similar epoxy-anhydride and acrylate systems [13,35,36] indicates that both curing stages are complete, as deduced from the results of FTIR analysis. Moreover the reaction heats of first and second curing stages are proportional to the amount of reactive species in the formulations. The Δh_{tot}, obtained for the global dynamic curing at 10 K/min (without UV irradiation), is close to the sum of Δh_1 and Δh_2,

suggesting the ability of LUP to promote the complete thermal free radical polymerization of acrylate groups.

Table 1. Reactions heat Δh_1 (stage 1, UV at 30 ºC), Δh_2 (stage 2, postcuring at 10 K/min after UV stage 1) and Δh_{tot}.(obtained at 10 K/min). T_g before and after each curing stage (*o*, *int* and ∞ indicate before stage 1, after stage 1 and after stage 2, respectively).

Formulation	T_{go} (ºC)	T_{gint} (ºC)	$T_{g\infty}$ (ºC)	Δh_1 (J/g)	Δh_2 (J/g)	Δh_1 (kJ/C=C)	Δh_2 (kJ/ee)	Δh_{tot} (J/g)
HT100	-70	52		378		107		377
HT25CEMA75	-67	16	82	271	95	102	113	380
HT50CEMA50	-64	-30	95	191	189	108	113	382
HT72CEMA25	-62	-43	116	94.5	282	107	112	377
CEMA100	-59		229		380		113	379

In general, it can be observed that T_g changes proportionally to the composition. The intermediate T_g (after acrylate polymerization) decreases with increasing CEMA content, due to the plasticizing effect of the liquid CEMA. For all formulations, a significant increase in T_g takes place during stage 2 due to the high rigidity of epoxy-anhydride network. Formulations HT25CEMA75 and HT50CEMA50 can be optimal candidates for 3D printing applications, with intermediate T_g below room temperature, low curing shrinkage during printing and higher final T_g, that ensures that rigid, glassy materials with high modulus at room temperature will be obtained upon completion of the dual-curing process [25].

4.2 Kinetic analysis

Photocuring of HTxCEMAy

First of all, the photocuring kinetics of HTxCEMAy set was examined. Figure 5 shows rate curves obtained from isothermal DCS runs at 30 ºC. As can be seen, within seconds upon irradiation, the photocuring of all formulations is complete with a very sharp curing profile. It was also verified that exposure to UV light did not produce any effect on the epoxy-anhydride, since dynamic postcuring after irradiation shows the same profile as the dual curing without light (see Figure 4). Heats of reaction (see Table 1) and FTIR analysis also confirm that acrylates react completely during photocuring, while no epoxide group reacts.

It can be observed in Figure 5 that the addition of CEMA to HT causes a decrease in the reaction rate during the photocuring stage, which is proportional to the HT content. Furthermore, the photocuring takes nearly the same time regardless of the CEMA content. These results could be partially explained taking into account that only the acrylates would react in the photocuring stage, while epoxy-anhydride groups would remain unreacted. However, the dilution effect caused by the addition of the CEMA component should be analyzed. One might expect that the mixture between HT and CEMA would produce a dilution of both the acrylate and the photo-initiator, and therefore a stronger decelerating effect might be expected. However, given that the dilution of HT facilitates light penetration [45], photolysis and photoinitiation rate would be somewhat enhanced, making up for the decrease in photo-initiator content (see Eq. 2).

A comparison between Figures 5 and 4 reveals the significant difference between thermal curing and phocuring rates of acrylates. The peak reaction rate for HT100 is close 60 W/g for UV activated reaction (at 30 ºC) and 6 W/g for thermal reaction (at temperatures greater than 100 ºC). Such a difference is explained by caused by the fast

release of active radicals upon photolysis of the photoinitiator in comparison the slower activation of the thermally latent LUP, which is also used at a low concentration.

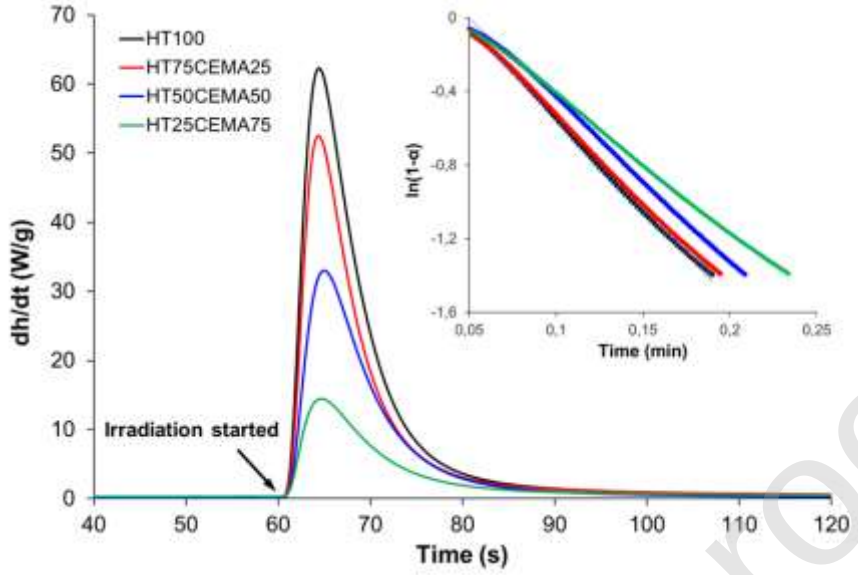

Figure 5. Reaction rate for the isothermal UV-curing at 30 °C of HTxCEMAy formulations. Inset shows logarithmic plots of unconverted fractions against time (the colour mapping is the same).

Inset of Figure 5 (ln(1-α) versus time) was created using Eq. (4), after a previous calculation of the conversion by integration of the calorimetric signal. The slopes of straight lines were used to calculate the first-order rate constant at 30 ºC for each formulation (see Table 2). As illustrated in Table 2, the polymerization rate slightly decreased with increasing CEMA content, but this decrease is lighter than expected, as was explained by the compromise between the dilutional effect of CEMA and the improvement in light penetration. Correlation coefficients show an excellent fit, which validate the methodology used.

Table 2. First-order rate constants and correlation coefficients for the photopolymerization of HTxCEMAy at 30 ºC

Formulation	k (min^{-1})	r
HT00	9.8	0.9992
HT75CEMA25	9.3	0.9993

HT50CEMA50	8.8	0.9992
HT25CEMA75	7.5	0.9995

Isothermal curing of HT100

In order to study the kinetics of thermally activated stage 1, HT100 was cured isothermally at 100, 110 and 120 °C for sufficiently long curing times to ensure completion of reaction. Figure 6 shows the resulting DSC traces.

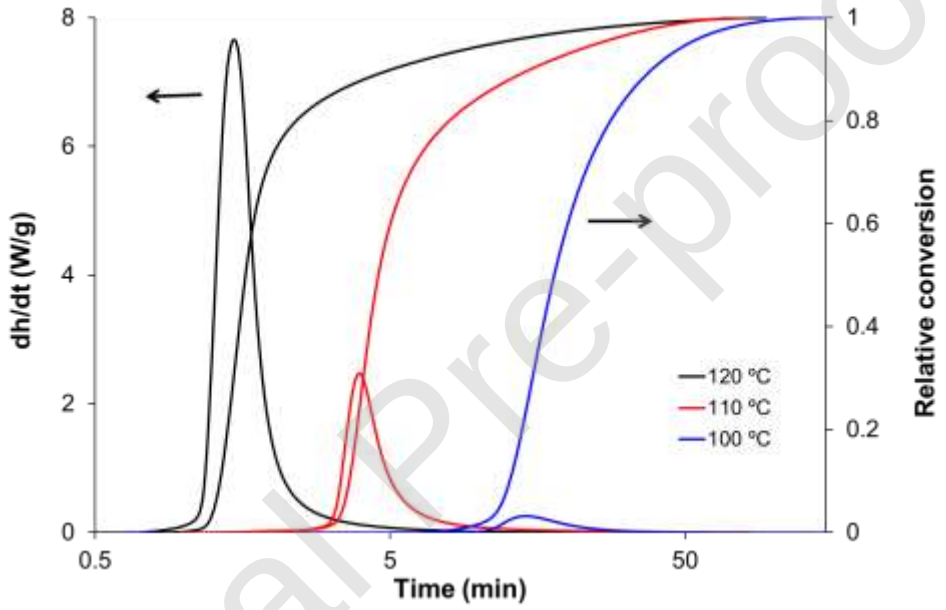

Figure 6. DSC traces and conversions of HT100 isothermally cured at different temperatures (stage 1).

The evolution of these curves with temperature follows expected trends, shifting to longer times on increasing the temperature. Curing behaviour is highly dependent on temperature, with a four-fold decrease in reaction rate with every 10 ºC drop of curing temperature. This suggests that the curing process is controlled by the decomposition of the initiator with high activation energy and not by propagation.

From the data shown in Figure 6 the kinetics of curing was established using isoconversional analysis and model fitting (autocatalytic model with $n + m = 2$) (Eqs. (5), (8) and (10)). Tables 3 and 4 show the results obtained. Activation energy and pre-

exponential factor are relatively constant throughout the curing, especially between 0.2 and 0.8 of fractional conversion, and similar to that obtained by model fitting. These results, along with the values of the regression coefficients confirm the reliability of the methodology and the kinetic parameters. It is observed that activation energies are of the same order of magnitude as other unsaturated systems cured by thermal activation of a radical initiator [34,46,47]. However, they are significantly higher than in systems where the initiator decomposes by the effect of a promoter [41].

Table 3. Kinetic parameters determined by isoconversional integral of isothermal stage 1 curing of HT100 (neat stage1)

α	E (kJ/mol)	$\ln\left[\frac{g(\alpha)}{A}\right]$ (min)	$\ln A^a$ (min^{-1})	r
0.1	137	-41.78	42.76	0.9988
0.2	140	-42.45	43.62	0.9983
0.3	142	-43.15	44.44	0.9980
0.4	144	-43.76	45.15	0.9977
0.5	147	-44.43	45.91	0.9977
0.6	149	-45.22	46.80	0.9982
0.7	152	-45.81	47.48	0.9992
0.8	148	-44.53	46.33	1.0000
0.9	122	-35.75	37.73	0.9989
Average	144	-43,36	44.84	0.9985

[a] Pre-exponential factor determined by using the isoconversional parameters and the autocatalytic model (see Table 4)

In order to compare the reactivities of the different curing stages and activation mechanisms, Table 4 also includes the rate constants at 30ºC and 150 ºC calculated using Arrhenius equation and model fitting activation energy and pre-exponential factor. The drastic change of $k_{30ºC}$ from $4.8 \cdot 10^{-6}$ min^{-1} for thermal activation to 9.8 min^{-1} for UV activation highlights the difference between the activation mechanisms and confirms that

adding LUP to the formulations does not jeopardize storage stability, since LUP is hardly reactive at 30 ºC.

Table 4. Kinetic parameters determined by model fitting analysis of isothermal stage 1 curing of HT100 (neat stage1)

n	m	E (kJ/mol)	$\ln A$ (min^{-1})	r	$k_{30ºC}$ [a] (min^{-1})	$k_{150ºC}$ [a] (min^{-1})
1.23	0.77	145	45.57	0.9953	$4.8 \cdot 10^{-6}$	61.8

[a] Rate constant k determined at 30 ºC and 150 ºC by using Arrhenius equation

Non-isothermal curing of CEMA100

The kinetics of curing of the neat formulation CEMA100 was studied. Due to the fact that CEMA100 has a very high T_g (229 ºC, see Table 1), the kinetics was studied under dynamic conditions to avoid the effect of vitrification during isothermal curing.

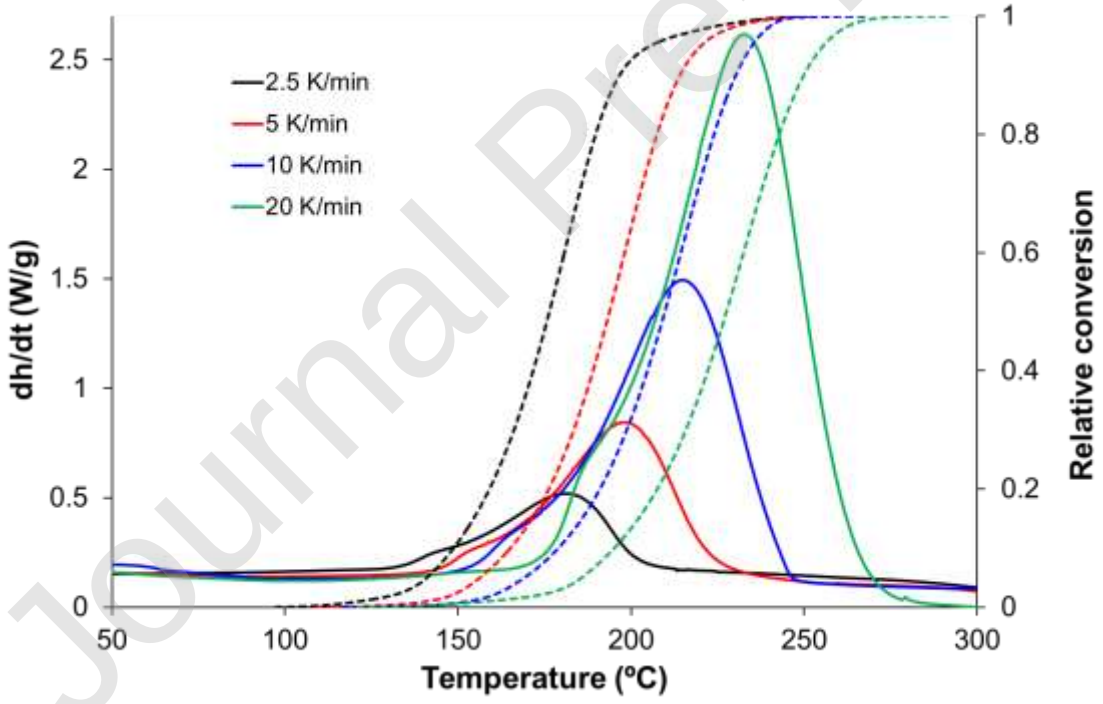

Figure 7. DSC thermograms (solid lines) and relative conversion (dashed lines) of CEMA100 at different heating rates

Figure 7 shows DSC traces and conversion-temperature plots of CEMA100 cured dynamically at different heating rates. As expected, the curves shift to higher

temperatures on increasing the heating rate. A slight effect of vitrification on the conversion curve at 2.5 K/min is observed, in agreement with previous results reported for neat CEMA formulations cured with 1-MI as initiator [35]. Compared to isothermal curing of HT100, CEMA100 cures at much higher temperatures, indicating that HTxCEMAy formulations can be cured using a temperature-controlled sequential dual-curing programme, as suggested by Figure 4.

Curing kinetics was established using Eq. (7) (isoconversional analysis) and Eqs. (9) and (10) with autocatalytic model with $n + m = 2$ (linear model fitting method), and the data shown in Figure 7. Table 5 and 6 show the isoconversional and model fitting kinetic parameters obtained, respectively. The quality of the fit is evident once more, from the constancy of the isoconversional parameters and the similarity of activation energies and pre-exponential factors obtained by both methods. The value of activation energy (ca. 69 kJ/mol) and the reaction orders are similar to those obtained for other epoxy-anhydride systems activated by a tertiary amine [35,36,48,49].

Table 5. Kinetic parameters determined by isoconversional integral of non-isothermal stage 2 curing of CEMA100 (neat stage2)

α	E (kJ/mol)	$\ln\left[\frac{AR}{g(\alpha)E}\right]$ (min)	$\ln\left[\frac{g(\alpha)}{A}\right]$ (min)	$\ln A^{a}$ (min^{-1})	r
0.1	67	7.84	-16.83	16.49	0.9986
0.2	67	7.38	-16.38	16.43	0.9986
0.3	68	7.20	-16.20	16.52	0.9990
0.4	68	7.10	-16.11	16.64	0.9992
0.5	69	7.03	-16.05	16.77	0.9994
0.6	69	6.97	-15.99	16.91	0.9995
0.7	70	6.91	-15.94	17.07	0.9995
0.8	70	6.86	-15.90	17.29	0.9996
0.9	72	7.08	-16.15	17.94	0.9995

Average	69	7.06	-16.06	16.90	0.9994

[a] Pre-exponential factor determined by using the isoconversional parameters and the autocatalytic model (see Table 6)

The lower k_{150^oC} for stage 2 (see Table 6) with respect to its value for thermal activated stage 1 (see Table 4) is a further confirmation of the sequential character of the thermal curing of HTxCEMAy mixtures. Moreover, during stage 1, epoxy groups hardly react. However, if one compares the constant at 30 ºC, k_{30^oC}, of HT100 (Table 4) and CEMA100 (Table 6), the trends are reversed. At low temperatures, DMAP activates the condensation of CEMA more effectively than LUP activates the free radical polymerization of acrylates. It is acknowledged that the rate constant *k* is a more reliable proxy to reactivity [50] than activation energy solely, because *k* combines the activation energy and the pre-exponential factor which may exert competing effects on curing rate. The radical acrylate homopolymerization of HT100 is controlled by the thermal decomposition of LUP, which has a high activation energy reflecting its latent character. In contrast, CEMA100 has a much lower activation energy because of the non-latent character of the initiator. Because of this, the curing process of HT100 slows down more drastically with decreasing temperature.

Table 6. Kinetic parameters determined by model fitting analysis of non-isothermal stage 2 curing of CEMA100

n	*m*	*E* (kJ/mol)	ln *A* (min^{-1})	*r*	k_{30^oC} [a] (min^{-1})	k_{150^oC} [a] (min^{-1})
1.48	0.52	68	16.75	0.9953	$2.5 \cdot 10^{-5}$	0.071

[a] Rate constant *k* determined at 30 ºC and 150 ºC by using Arrhenius equation

Non-isothermal dual curing of HT50CEMA50

HT50CEMA50 formulation was selected to study the dual-curing. Figure 8 shows conversions and DSC curves at different heating rates. Again, the evolution of these curves follows the expected trends, shifting to higher temperatures on increasing the

heating rate. Although the curing seems highly sequential, some overlapping of stages is observed, which may affect the determination of the kinetic parameters.

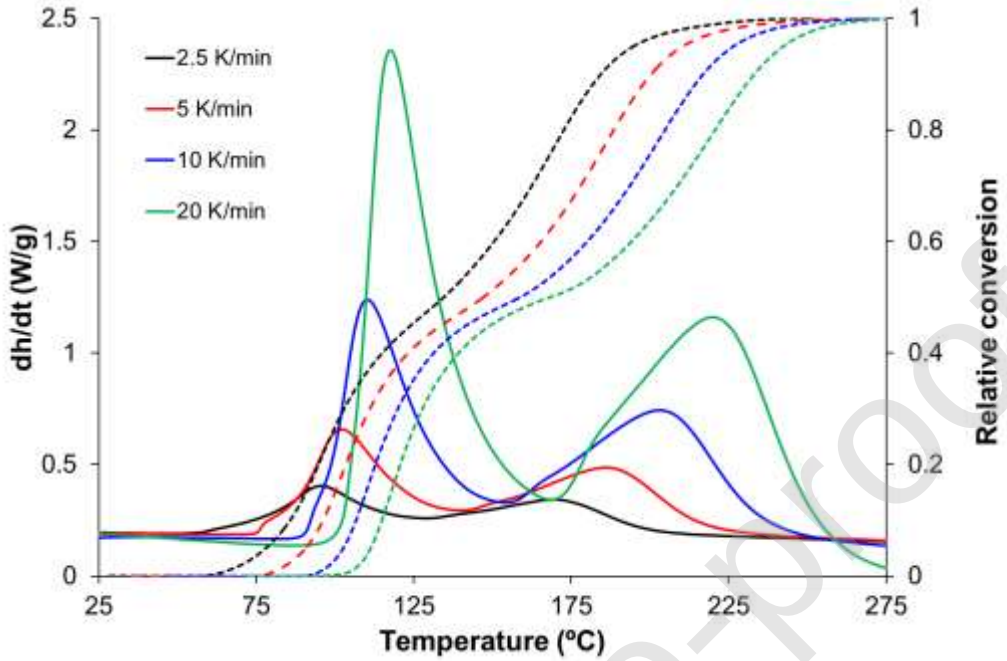

Figure 8. DSC thermograms (solid lines) and relative conversion (dashed lines) of HT50CEMA50 at different heating rates

Table 7 and 8 show the kinetic data obtained by isoconversional and model fitting methods, respectively. Isoconversional data at 0.5 are not included due to the slight overlap between stages in this region. This conversion represents the transition between stages. The results reported in these tables confirm the significant difference between the kinetics of the two curing stages. The kinetic parameters of stage 2 are similar to those obtained for neat CEMA (see Tables 5 and 6), although *k* shows a slight increase in the dual formulation, in accordance with the data shown in Figure 4 and accompanying discussion. Stage 1 activation energy of the dual formulation decreases in comparison to the neat HT100 due to the lower activation energy of the redox decomposition of LUP promoted by DMAP [41,46]. The comparison of the rate constants *k* at 30ºC and 150ºC between neat stage 1 (see Table 4) and the dual-curing shows that the accelerating effect

of DMAP dominates at low temperature, and the dilutional effect of CEMA dominates at high temperature.

Table 7. Kinetic parameters determined by isoconversional integral non-isothermal curing of HT50CEMA50

α	E (kJ/mol)	$\ln\left[\frac{AR}{g(\alpha)E}\right]$ (min)	$\ln\left[\frac{g(\alpha)}{A}\right]$ (min)	$\ln A$ [a] (min^{-1})	r
0.1	75	14.39	-16.59	22.61	0.9966
0.2	89	18.26	-20.63	27.43	0.9988
0.3	98	20.24	-22.70	30.16	0.9993
0.4	108	22.31	-24.87	33.11	0.9996
0.45	108	21.56	-24.13	33.02	0.9969
Average 1	91	19.35	-21.78	29.26	0.9988
0.55	72	9.67	-11.83	19.40	0.9991
0.6	71	8.91	-11.05	18.75	0.9989
0.7	71	8.27	-10.41	18.35	0.9993
0.8	71	7.92	-10.07	18.33	0.9995
0.9	74	8.10	-10.29	19.01	0.9996
Average 2	72	8.57	-10.73	18.77	0.9993

[a] Pre-exponential factor determined by using the isoconversional parameters and the autocatalytic model. g(α) was determined using relative conversion from 0 to 1 for each stage

Table 8. Kinetic parameters determined by model fitting analysis of both stages of HT50CEMA50

n	m	E (kJ/mol)	$\ln A$ (min^{-1})	r	k_{30^oC} [a] (min^{-1})	k_{150^oC} [a] (min^{-1})
Stage 1						
1.80	0.20	92	28.30	0.9938	$2.7\cdot10^{-4}$	8.4
Stage 2						
1.58	0.42	72	17.87	0.9992	$2.7\cdot10^{-5}$	0.084

[a] Rate constant k determined at 30 ºC and 150 ºC by using Arrhenius equation

Stage 2 non-isothermal curing of HT50CEMA50

To study the second stage of dual-curing without any overlapping of stage 1, HT50CEMA50 formulation has been dynamically cured at different heating rates after being photocured at 30 °C. Figure 9 shows heat flows and conversions versus temperature at different heating rates. As expected, the DSC peak appeared at the same temperature zone as stage 2 of non-isothermal dual-curing (see Figure 4). On the heat flow curves given in Figure 9, shoulders can be seen at the low temperature region associated to DMAP activation, similar to what was observed in previous works [51]. This shoulder is also observed in dual-curing (see Figure 8) albeit not clearly due to the slight overlap between stages.

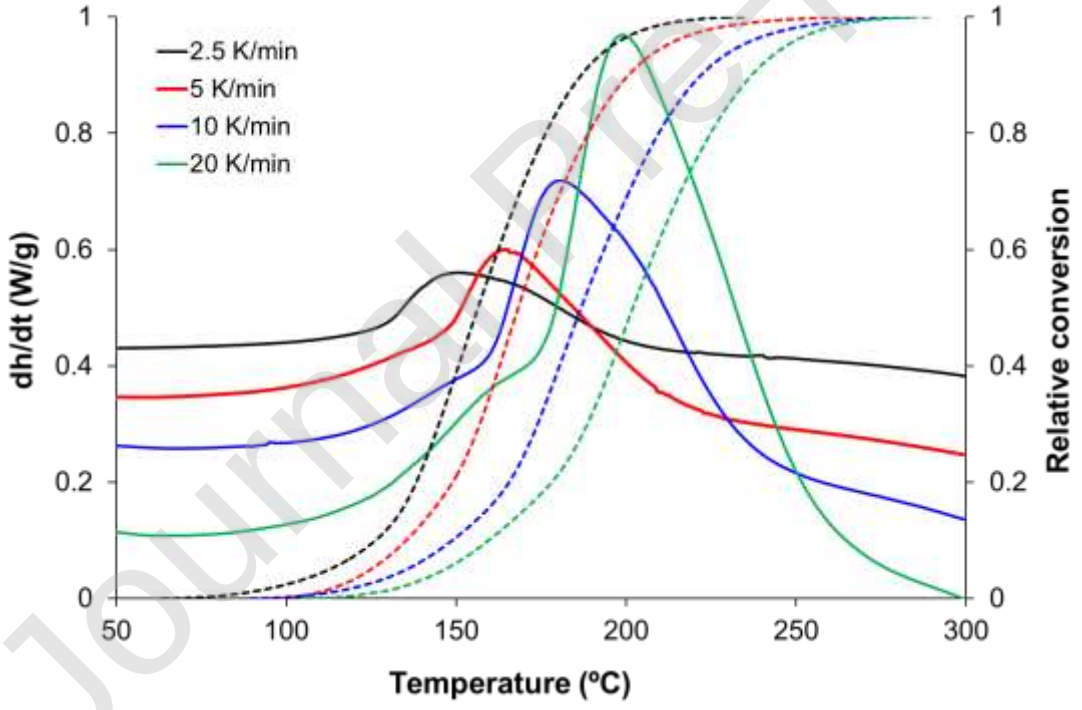

Figure 9. DSC thermograms (solid lines) and relative conversion (dashed lines) of HT50CEMA50 at different heating rates after photocuring at 30 ºC.

Table 9 and 10 present kinetic parameters obtained from the curves in Figure 9. Isoconversional parameters are relatively constant throughout the whole conversion range

except at the beginning of curing when initiator activation slightly increases activation energy and pre-exponential factor. The kinetic parameters are similar to those obtained for stage 2 in thermal dual-curing (see Tables 7 and 8) and neat CEMA100 (see Table 5 and 6). Nevertheless, the reactivity of stage 2 of HT50CEMA50 formulation is slightly higher than that of the neat CEMA100, as discussed above. Isothermal curing at 120-190 ºC (after UV irradiation at 30 ºC) was also studied (results not shown) and the kinetics data produced were similar to those shown in Tables 9 and 10, but poor regression coefficients were obtained due to the difficulty in obtaining reliable kinetic data and their analysis.

Table 9. Kinetic parameters determined by isoconversional integral analysis of non-isothermal stage 2 curing of HT50CEMA50 (neat stage 2 after stage 1 UV).

α	E (kJ/mol)	$\ln\left[\frac{AR}{g(\alpha)E}\right]$ (min)	$\ln\left[\frac{g(\alpha)}{A}\right]$ (min)	$\ln A^{a}$ ($\ln$ min^{-1})	r
0.1	80	13.20	-22.38	21.16	0.9973
0.2	71	9.66	-18.72	18.07	0.9966
0.3	68	8.32	-17.33	17.07	0.9983
0.4	67	7.98	-16.98	17.03	0.9980
0.5	68	7.83	-16.84	17.18	0.9970
0.6	68	7.68	-16.69	17.32	0.9959
0.7	69	7.47	-16.49	17.44	0.9954
0.8	69	7.25	-16.28	17.61	0.9957
0.9	70	7.01	-16.05	17.96	0.9939
Average	70	8.39	-17.42	17.76	0.9963

[a] Pre-exponential factor determined by using the isoconversional parameters and the autocatalytic model

Table 10. Kinetic parameters determined by model fitting analysis of non-isothermal stage 2 curing of HT50CEMA50 (neat stage 2 after stage 1 UV)

n	m	E (kJ/mol)	$\ln A$ (min^{-1})	r	k_{30^oC} [a] (min^{-1})	k_{150^oC} [a] (min^{-1}) [b]
1.71	0.29	70	17.70	0.9963	$5.0 \cdot 10^{-5}$	0.125

[a] Rate constant k determined at 30 ºC and 150 ºC by using Arrhenius equation

The kinetic parameters obtained in this section seem to be the most accurate for stage 2 so far. This is because the overlap at around the fractional conversion of 0.5 in thermal dynamic dual curing and the problems of heat detection in isothermal curing are avoided. Therefore, this methodology will be used to compare the kinetics of stage 2 among the different dual HTxCEMAy formulations.

Kinetic parameters of thermal curing of HTxCEMA formulations

In this section we compare the dual-curing kinetics of all formulations. The detailed study of the curing kinetics of HT100, CEMA100 and HT50CEMA50 were described in previous sections. HT25CEMA75 and HT75CEMA25 were studied in the same way as HT50CEMA50, and the results obtained were qualitatively similar to those of HT50CEMA50.

Table 11 shows the results obtained by model fitting which were equivalent to the results of isoconversional analysis. For dual formulations, whereas stage 1 kinetic data were obtained by non-isothermal curing, without separating the two stages by deconvolution, stage 2 data were obtained by non-isothermal postcuring of irradiated formulations. Results of neat formulations HT100 and CEMA100 were also included to facilitate comparison.

Table 11 Kinetic parameters determined by model fitting analysis of all HTxCEMAy formulations studied.

Formulation	*n*	*m*	*E* (kJ/mol)	ln *A* (min^{-1})	*r*	k_{150^oC} [a] (min^{-1})
			Stage 1			
HT100	1.23	0.77	145	45.47	0.9952	61.8
HT75CEMA25	1.65	0.35	128	39.53	0.9984	23.2
HT50CEMA50	1.80	0.20	92	28.30	0.9938	8.4
HT25CEMA75	1.76	0.224	78	24.18	0.9983	6.6
			Stage 2			
HT75CEMA25	1.61	0.39	64	15.93	0.9981	0.139
HT50CEMA50	1.71	0.29	70	17.70	0.9963	0.125
HT25CEMA75	1.65	0.35	71	17.93	0.9997	0.117
CEMA100	1.48	0.52	68	16.74	0.9995	0.071

[a] Rate constant *k* determined at 150 ºC by using Arrhenius equation

Activation energy and the rest of the kinetic parameters change regularly with composition. Activation energy of the first curing stage decreases from 145 kJ/mol to 78 kJ/mol because of the effect of the redox mechanism promoted by DMAP on the decomposition of LUP and activation of the radical polymerization. At higher temperatures the reaction rate increases significantly on increasing the HT content, as indicated by k_{150^oC}, because of the higher activation energy of the purely thermal decomposition mechanism. Second stage kinetic parameters are relatively constant, but the kinetic constants clearly reflect the change in reactivity with changing HT content, as discussed above. The kinetic data also confirms the sequential dual character of HTxCEMAy formulations, with significantly higher k_{150^oC} at stage 1 compared to stage 2.

Figure 10 features the Arrhenius plot of ln*k* versus the inverse of temperature, obtained using activation energies and pre-exponential factors from Table 11. ln*k* at 30 ºC of the photocuring is also included (filled triangle).

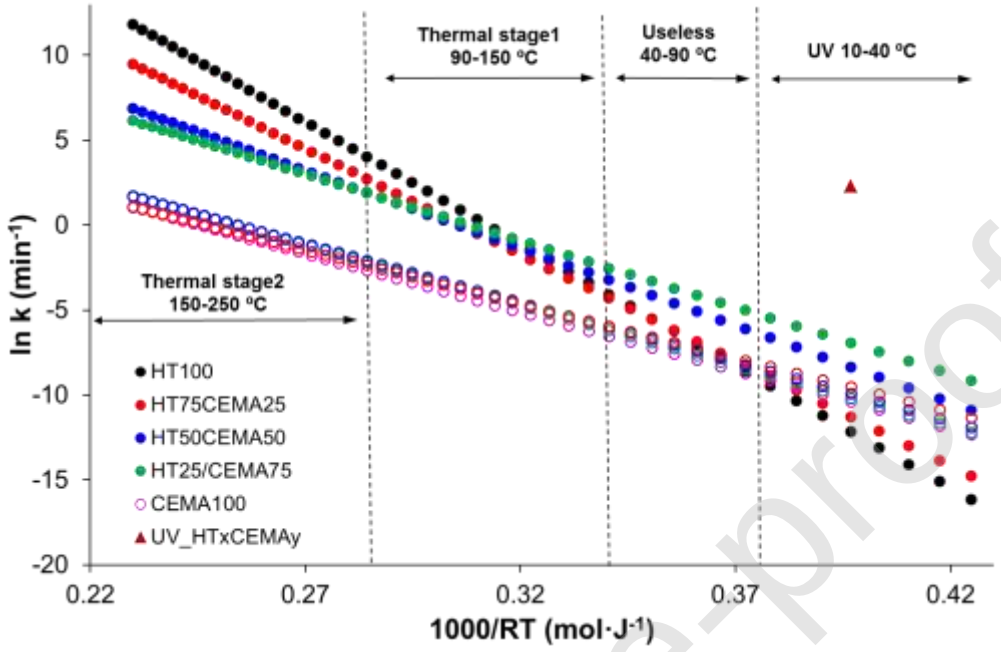

Figure 10. Arrhenius plot, ln*k* versus 1000/RT for all formulations and curing stages studied. Thermal stage 1 and stage 2 are represented with filled and empty circles respectively, with the same colors.

The Arrhenius plot is divided in four thermal sections with different reactivities: a) UV region at low temperatures where only HT polymerization takes places, b) a useless region where both stages do not react in a reasonable time frame, c) a region where HT reacts thermally and CEMA could react but extremely slowly and d) a thermal region at higher temperatures where CEMA reacts conveniently and HT very quickly. Region "d" is the most convenient for postcuring of dual 3D printing systems, since it ensures a complete stage 2 and completely reacted acrylates which otherwise remain not fully reacted after 3D printing. This plot also indicates that, although the curing can be carried out sequentially given proper selection of stage temperatures, the situation may change upon storage at low temperatures. This is because, at such low temperatures, the kinetic constant of the thermally activated radical polymerization and the epoxy-anhydride

copolymerization become similar in magnitude, in spite of the extrapolation error. This suggests that prolonged storage at room temperature might result in the activation of the epoxy-anhydride reaction in the first place, instead of the radical acrylate polymerization.

All in all, Figure 10 provides an exhaustive summary of the hitherto kinetic discussions, and it achieves this without losing its intuitive appeal. The intersecting Arrhenius plots featured in the figure suggest once more that a simple interpretation of reaction rate based on the assumption that a low activation energy implies a faster reaction, may prove wrong depending on the value of pre-exponential factor and on reaction conditions. However, it also shows that the difference in activation energy does have a significant effect on the temperature dependence of the different processes, and this can be taken to advantage in the design of safe curing procedures for dual curing systems such as the one presented in this work or other systems [43].

Simulation of the curing

Simulation of the curing is a powerful tool when the conversions are difficult to obtain experimentally or when curing times are extremely long. Figure 3 shows the good fit between the experimental data of stage 2 (170 ºC) of HT50CEMA50 formulation and the simulation using the non-isothermal data in Table 9. This is an expected result as long as the simulation is performed within the experimental data range, whether the data is isothermal or dynamic.

Good storage stability is essential for commercial 3D printing formulations, since the prepared formulations are usually stored at room temperature. In this section, the results from our 50-day stability tests are presented. Uncured samples HT50CEMA50 were stored in an oil bath at 20ºC and the daily evolution of T_g and residual heat were monitored by performing dynamic DSC scans at 10 K/min. The loss of stability is manifested as a

decrease in residual heat, accompanied by an increase in T_g. Using residual heats, the loss of storage stability could be quantified as an increase of conversion.

Figure 11 shows some DSC postcuring thermograms at different storage times. A slight increase in T_g and a slight decrease in stage 2 heat flow peak intensity can be observed. Observing the figure, one can note that the initial peak (associated to acrylate homopolymerization) remains unchanged in 50 days. Therefore, one can safely postulate that at 20 ºC, LUP cannot decompose and that only DMAP, although very slowly, is able to activate stage 2. In accordance with this idea, the evolution of the conversion during stability was simulated, considering that only stage 2 is plausible during storage. The evolution of relative stage 2 conversion during storage at 20 ºC was evaluated as:

$$\alpha = \frac{\left(\Delta h_{tot} - \Delta h_{res}\right)\cdot 2}{\Delta h_{tot}} \qquad (12)$$

where Δh_{tot} is the total reaction heat at 10 K/min, Δh_{res} is residual heat at 10 K/min after different storage times. The factor of 2 is used to transform absolute conversion to relative conversion (HT50CEMA50 formulation).

The inset of Figure 11 shows the stage 2 relative conversion as a function of storage time. It can be observed that the formulation is relatively stable during the first 20 days. An increase in conversion is observed afterwards. In either case, after 50 days, the formulation is still far from its gel point and as such, still apt for 3D printing.

To perform the simulation, the isoconversional parameters given in Table 9 were extrapolated at 20 ºC. The relatively good fit supports the earlier postulation and it validates the simulation methodology used (see inset Figure 11).

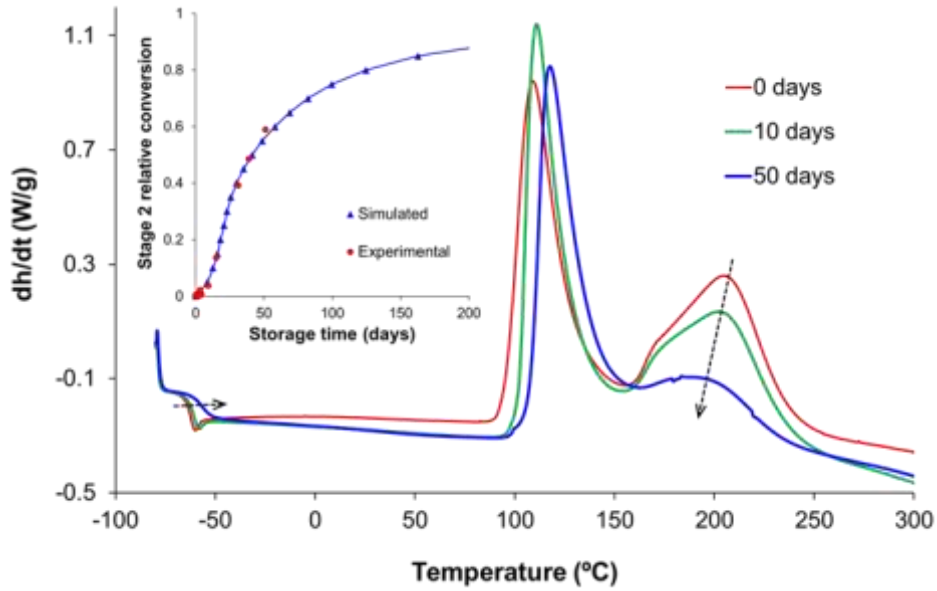

Figure 11. Evolution of T_g and residual heat of HT50CEMA50 during stability test at 20 ºC. Inset shows the stage 2 conversion versus storage time.

5 Conclusions

In this work, the curing kinetics of a new family of dual-curable thermosets was analysed. The curing takes place sequentially in two steps: acrylate polymerization by UV light or by thermal activation; followed by thermal epoxy-anhydride curing. Photocuring kinetics was satisfactorily represented by a first order model and the thermal curing was studied by isoconversional and model fitting methodologies.

The dual nature of the curing process has been proven both directly by experiments and also indirectly by analysing the kinetic parameters. Experimentally, the use of a thermally triggered radical initiator ensured full acrylate conversion which was otherwise not achievable solely by photopolymerization in 3D printing. Although formulations are intended for stereolithography, the addition of the thermal radical initiator amplifies the domain of application for these thermosets and facilitates their preparation through conventional and purely thermal procedures.

The use of the activation energy alone to establish the reactivity may lead to errors. It is safer to use the rate constant which incorporates the effect of both the activation

energy and the pre-exponential factor. Within the conventional temperature range of the dual-curing, it has been proven that the acrylate photocuring rate constant is one order of magnitude higher than its thermal counterpart, and fifty times higher than epoxy-anhydride condensation rate.

The isoconversional methodology used herein is a useful and simple tool that allows a comprehensive analysis of kinetics without requiring any well-defined kinetic model. It enables one to simulate the curing process, even at temperatures way out of the experimental range.

Author Statement

X. Ramis, X. Fernández-Francos, O. Konuray: Conceptualization, Methodology, Software. **X. Ramis, X. Fernández-Francos, O. Konuray, J.M. Salla**: Data curation, Writing- Original draft preparation. **J.M. Morancho, O. Konuray, M. García-Alvarez**: Visualization, Investigation. **X. Ramis**: Supervision. **X. Ramis, O. Konuray:** Writing-Reviewing and Editing. **X. Ramis:** Project administration

Declaration of interests

The authors declare that they have no known competing financial interests or personal relationships that could have appeared to influence the work reported in this paper.

Acknowledgments

The authors would like to thank MCIU (Ministerio de Ciencia, Innovación y Universidades) (MAT2017-82849-C2-1-R and MAT2017-82849-C2-2-R), FEDER (Fondo Europeo de Desarrollo Regional) (MAT2017-82849-C2-1-R, MAT2017-82849-C2-2-R and BASE3D) and Generalitat de Catalunya-Secretaria d'Universitats i Recerca (BASE3D, 2017-SGR-77 and Serra Húnter program) for the financial support. We also thank Spot-A Materials for supplying the Spot-HT.

References

[1] C. Sun, N. Fang, D.M. Wu, X. Zhang, Projection micro-stereolithography using digital micro-mirror dynamic mask. Sensors and Actuators, A: Physical, 121 (2005), 113-120. https://doi.org/10.1016/j.sna.2004.12.011.

[2] S.C. Ligon, R. Liska, J. Stampfl, M. Gurr, R. Mülhaupt, Polymers for 3D printing and customized additive manufacturing, Chemical Reviews 117 (2017), 10212-10290. https://doi.org/10.1021/acs.chemrev.7b00074.

[3] M. Hofmann, 3D printing gets a boost and opportunities with polymer materials. ACS Macro Letters, 3 (2014) 382-386. https://doi.org/10.1021/mz4006556.

[4] C. Evans, E. Taneva, B. Kusnoto, 3D Scanning, Imaging, and Printing in Orthodontics, in: S. Narett (Ed.), Issues in Contemporary Orthodontics, Ch. 9, Publisher: Intech Editors, 2015. doi: 10.5772/60010.

[5] P. Makvandi, C.Esposito, F. Paladini, A.L. Gallo, F. Montagna, R. Jamaledin, M. Pollini, A. Maffezzoli, Antimicrobial modified hydroxyapatite compositedental bite by stereolithography, Polym. Adv. Tech. 29 (2018) 364-371.https://doi.org/10.1002/pat.4123.

[6] F.J.O'Brien, Biomaterials & scaffolds for tissue engineering, Materials Today, 14 (2011) 88-95. https://doi.org/10.1016/S1369-7021(11)70058-X.

[7] M.A. Przeradzka M. A., B. van Bochove, T.C. Bor, D.W. Grijpma, Phase-separated mixed-macromer hydrogel networks and scaffolds prepared by stereolithography, Polym. Adv. Tech. 28 (2017) 1212-1218. https://doi.org/10.1002/pat.3916.

[8] S.-Z. Guo, K. Qiu, F. Meng, S.H. Park, M.C. McAlpine, 3D Printed Stretchable Tactile Sensors, Adv. Mater. 29 (2017) 1701218. https://doi-org.recursos.biblioteca.upc.edu/10.1002/adma.201701218.

[9] G.J. Pagan-Diaz, X. Zhang, L. Grant, Y. Kim, O. Aydin, C. Cvetkovic, E. Ko, E. Solomon, Simulation and Fabrication of Stronger, Larger, and Faster Walking Biohybrid Machines, Adv. Func. Mat. 28 (2018) 1801145. https://doi.org/10.1002/adfm.201801145.

[10] D. Kokkinis F, Bouville A.R. Studart, 3D Printing of Materials with Tunable Failure via Bioinspired Mechanical Gradients, Adv. Mater. 30 (2018) 17505808. https://doi.org/10.1002/adma.201705808.

[11] R.U. Hassan, J. Seok, Fabrication of a functionally graded and magnetically responsive shape memory polymer using a 3D printing technique and its characterization, J. Appl. Polym. Sci., 135 (2018),45997/1-45997/7. https://doi.org/10.1002/app.45997.

[12] V. Muccia, G. Arenas, R. Duchowic, W.D, Cook, C. Vallo, Influence of thermal expansion on shrinkage during photopolymerization of dental resins based on bis-GMA/TEGDMA, Dental Materials, 25 (2009) 103-114. https://doi.org/10.1016/j.dental.2008.04.014.

[13] A.C. Uzcategui, A.Muralidharan, V.L. Ferguson, S.J. Bryant, R.R. McLeod, Understanding and Improving Mechanical Properties in 3D printed Parts Using a Dual-Cure Acrylate-Based Resin for Stereolithography, Adv. Eng. Mater. 20 (2018) 1800876. https://doi.org/10.1002/adem.201800876.

[14] A. Gupta, A.A. Ogale, Dual curing of carbon fiber reinforced photoresins for rapid prototyping, Polym. Com. 23 (2002) 1162-1170. https://doi.org/10.1002/pc.10509.

[15] C. Esposito Corcione, R. Striani, F. Montagna, D. Cannoletta, Organically modified montmorillonitepolymer nanocomposites for stereolithography building process, Polym. Adv. Tech., 26, 92–98 (2015). https://doi.org/10.1002/pat.3425.

[16] J. Bonada, A. Muguruza, X. Fernández-Francos, X. Ramis, Influence of exposure time on mechanical properties and photocuring conversion ratios for photosensitive materials used in Additive Manufacturing, Procedia Manufacturing 13 (2017) 762-769. https://doi.org/10.1016/j.promfg.2017.09.18.

[17] O. Konuray, F. Di Donato, M. Sangermano, J. Bonada, A. Tercjak, X. Fernández-Francos, À. Serra, X. Ramis, Dual-curable stereolithography resins for superior thermomechanical properties, Express Polym. Lett. 14 (2020). https://doi.org/10.3144/expresspolymlett.2020.72.

[18] J.M. Morancho, X. Fernández-Francos, X. Ramis, J.M. Salla, A. Serra, Photocuring and thermal post-curing of a cycloaliphatic epoxide resin with a trithiol and a vinyl epoxy

compound, J. Therm. Anal. Calorim. 121 (2015) 389-395. doi: 10.1007/s10973-015-4535-y.

[19] G.F. Arenas, R. Duchowicz, Vitrification of photo-curing resins by embedded cantilever and Fizeau interferometer, Proceedings Volume 8011, 22nd Congress of the International Commission for Optics: Light for the Development of the World, 80114Y (2011) doi: 10.1117/12.902194

[20] D.A. Abu-elenain, S.H. Lewis, J.W. Stansbury, Property evolution during vitrification of dimethacrylate photopolymer networks, Dental Materials 29 (2013) Pages 1173-118. https://doi.org/10.1016/j.dental.2013.09.002.

[21] S.C. Ligon, B. Husár, H. Wutzel, R. Holman, R. Liska, Strategies to reduce oxygen inhibition in photoinduced polymerization, Chem. Rev. 114 (2014) 557-589. https://doi.org/10.1021/cr3005197.

[22] G. González, X. Fernández-Francos, A. Serra, M. Sangermano, X. Ramis, Environmentally-friendly processing of thermosets by two-stage sequential aza-Michael addition and free-radical polymerization of amine–acrylate mixtures, Polym. Chem. 6 (2015) 6987-6997.

[23] G. Griffini, M. Invernizzi, M. Levi, G. Natale, G. Postiglione, S. Turri, 3D-printable CFR polymer composites with dual-cure sequential IPNs. 91 (2016) 174-179. https://doi.org/10.1016/j.polymer.2016.03.048.

[24] X. Kuang, Z. Zhao, K. Chen, D. Fang, G. Kang, H.J. Qi, High-Speed 3D Printing of High-Performance Thermosetting Polymers via Two-Stage Curing, Macromol. Rapid. Commun. 39 (2018) 1700809. https://doi.org/10.1002/marc.201700809.

[25] O. Konuray, A. Altet, X. Fernández-Francos, X. Ramis, Epoxy-doped poly-acrylate 3D printed materials with nanoscale phase separation. (2020) submitted.

[26] K. Dean, W.D. Cook, Effect of curing sequence on the photopolymerization and thermal curing kinetics of dimethacrylate/epoxy interpenetrating polymer networks. Macromolecules 35 (2002) 7942-7954. https://doi.org/10.1021/ma020628p.

[27] K. Dean, W.D. Cook, M.D. Zipper, P. Burchill, Curing behaviour of IPNs formed from model VERs and epoxy systems I amine cured epoxy. Polymer 42 (2001) 1345-1359. https://doi.org/10.1016/S0032-3861(00)00486-9..

[28] K. Dean, W.D. Cook, P. Burchill, P., M. Zipper, Curing behaviour of IPNs formed from model VERs and epoxy systems: Part II. Imidazole-cured epoxy. Polymer, 42 (2001) 3589-3601. https://doi.org/10.1016/S0032-3861(00)00745-X.

[29] O. Konuray, J.M. Salla, J.M. Morancho, X. Fernández-Francos, M. García-Alvarez, X. Ramis, Time-temperature-transformation (TTT) diagram of dual-curable epoxy thermosets obtained via two sequential epoxy-amine condensations, Thermochim. Acta 678 (2019) 178305, https://doi.org/10.1016/j.tca.2019.178305.

[30] N. Areny, O. Konuray, X. Fernàndez-Francos, J.M. Salla, J.M. Morancho, X. Ramis, Time-temperature-transformation (TTT) diagram of a dual-curable off stoichiometric epoxy-amine system with latent reactivity, Thermochim. Acta, 666 (2018) 124-134. https://doi.org/10.1016/j.tca.2018.06.012.

[31] C. Decker, Kinetic Study and New Applications of UV Radiation Curing, Macromol. Rapid Commun. 23 (2002) 1067-1093. http://dx.doi.org/10.1002/marc.200290014.

[32] J.-S. Kim, .S.-T. Noh, J.-O. Kweon, B.-S. Cho, Photopolymerization kinetic studies of UV-curable sulfur-containing difunctional acrylate monomers using photo-DSC, Macromol. Research. 23 (2015) 341-349.

[33] S. Vyazovkin, A.K. Burnham, J.M. Criado, L.A. Pérez-Maqueda, C. Popescu, N. Sbirrazzuoli ICTAC Kinetics Committee recommendations for performing kinetic computations on thermal analysis data, Thermochim. Acta 520 (2011) 1-19. doi:10.1016/j.tca.2011.03.034.

[34] A. Cadenato, J. M. Morancho, X. Fernández-Francos, J. M. Salla, X. Ramis, Comparative kinetic study of the non-isothermal thermal curing of bis-GMA/TEGDMA systems, J. Thermal Anal. Cal. 89 (2007) 233-244. https://doi.org/10.1007/s10973-006-7567-5.

[35] A. Belmonte, F. Dabritz, X. Ramis, A. Serra,B. Voit, X. Fernandez-Francos, Cure Kinetics Modeling and Thermomechanical Properties of Cycloaliphatic Epoxy-Anhydride

Thermosets Modified With Hyperstar Polymers, J. Polym. Sci. Parta B: Polym. Phys. 52 (2014) 1227-1242. doi: 10.1002/polb.23555.

[36] M. Flores, X. Fernández-Francos, X. Ramis, A. Serra, Novel epoxy-anhydride thermosets modified with a hyperbranched polyester as toughness enhancer. I. Kinetics study, Thermochim. Acta 544 (2012) 17-26. http://dx.doi.org/10.1016/j.tca.2012.06.00

[37] T. Akahira, T. Sunose, Method of determining activation deterioration constant of electrical insulating materials, Res. Report Chiba Inst. Technol. (Sci. Technol.) 16 (1971) 22-31.

[38] A.W. Coats and J.P. Redfern, Kinetic Parameters from Thermogravimetric Data, Nature 207 (1964) 68-69. http://dx.doi.org/10.1038/201068a0.

[39] F. Shokrolahi, M. Zandi, P. Shokrollah, M. Atai, E. Ghafarzadeh, M. Hanifeh, Cure kinetic study of methacrylate-POSS copolymers for ocular lens, Pro. Biomater. 6 (2017) 147-156. https://doi.org/10.1007/s40204-017-0074-x.

[40] J. Masson Acrylic Fiber Technology and Applications CRC Press, Cleveland 1995.

[41] J.M. Salla, X. Ramis, A Kinetic Study of the Effect of Three Catalytic Systems on the Curing of an Unsaturated Polyester Resin, J. Appl. Polym. Sci., 51 (1994) 453-462. https://doi.org/10.1002/app.1994.070510308

[42] B.Vazquez, B. Levenfeld, J. San Roman, Role of Amine Activators on the Curing Parameters, Properties and Toxicity of Acrylic Bone Cements, Polym. Int., 46 (1998) 241-250. https://doi.org/10.1002/(SICI)1097-0126(199807)46:3<241::AID-PI49>3.0.CO;2-G

[43] C. Russo, M.A. Serra, X. Fernandez-Francos, S. de la Flor, Characterization of sequential dual-curing of thiol-acrylate-epoxy systems with controlled thermal properties, Eur. Polym. J. 112 (2019) 376-388. https://doi.org/10.1016/j.eurpolymj.2018.12.048.

[44] A. Bonnet, J. P. Pascault, H. Sautereau, M. Taha, Y. Camberlin, Epoxy-Diamine Thermoset/Thermoplastic Blends. 1. Rates of Reactions before and after Phase Separation, Macromolecules 32 (1999) 8517-8523. https://doi.org/10.1021/ma981754p

[45] G.A. Miller, L. Gou, V. Narayanan, A.B. Scranton, Modeling of photobleaching for the photoinitiation of thick polymerization systems, J. Polym. Sci. Part A Polym. Chem. 40 (2002) 793-808. http://dx.doi.org/10.1002/pola.10162.

[46] J.M. Salla, X. Ramis, Comparative Study of the Cure Kinetics of an Unsaturated Polyester Resin Using Different Procedures, Polym. Eng. Sci. 36 (1996) 835-851. https://doi.org/10.1002/pen.10471.

[47] J. M. Morancho, A. Cadenato, X. Fernández-Francos, J. M. Salla and X. Ramis, Isothermal kinetics of photopolymerization and thermal polymerization of bis-GMA/TEGDMA resins, J. Thermal. Anal. Cal. 92 (2008) 513-522. doi: 10.1007/s10973-007-8432-x.

[48] J.M. Morancho, X. Fernández-Francos, C. Acebo, X. Ramis, J.M. Salla, A Serra, Thermal curing of an epoxy-anhydride system modified with hyperbranched poly(ethylene imine)s with different terminal groups, J. Therm. Anal. Calorim. 127 (2017) 645-654. doi: 10.1007/s10973-016-5376-z.

[49] S. Montserrat, G. Andreu, P. Cortés, Y. Calventus, P. Colomer, J.M. Hutchinson, J. Malek, Addition of a reactive diluent to a catalyzed epoxy-anhydride system. I. Influence on the cure kinetics, J Appl Polym Sci. 61 (1996) 1663-674. https://doi.org/10.1002/(SICI)1097-4628(19960906)61:10<1663::AID-APP6>3.0.CO;2-E.

[50] S. Vyazovkin, C.A. Wight, Kinetic in solids, Annu. Rev. Phys. Chem. 48 (1997) 125-149. https://doi.org/10.1146/annurev.physchem.48.1.125.

[51] O. Konuray, N. Areny, J.M. Morancho, X. Fernández-Francos, A.Serra, X. Ramis, Preparation and characterization of dual-curable off-stoichiometric amine-epoxy thermosets with latent reactivity, Polymer 146 (2018) 42-52. https://doi.org/10.1016/j.polymer.2018.05.040.